Application of Loop-Flower Basis Functions in the Time-Domain Electric Field Integral Equation

Xuezhe Tian, Gaobiao Xiao, and Jinpeng Fang

***Abstract*—The loop-flower basis functions are applied to get a low-frequency stable time-domain electric field integral equation (TD-EFIE). The quasi-Helmholtz decomposition is performed by the loop-flower basis functions, which are all defined based on mesh nodes. To get a well-posed equation, a temporally differentiated form of the TD-EFIE is tested with the flower function and the undifferentiated form is tested with the loop function. For a robust MOT solver, the averaging scheme is also adopted to alleviate the high-frequency instabilities. Numerical verifications of perfect electric conductor (PEC) transient scattering problems are provided to demonstrate the accuracy and stability of the proposed technique.**

***Index Terms*—Helmholtz decomposition, loop-flower, low-frequency instability, marching on in time (MOT), time-domain electric field integral equation (TD-EFIE).**

I. Introduction

Time-domain integral equations (TDIEs) have kept an increasing appeal in the computational electromagnetic (CEM) for their applications in large scale and complex structures, wideband problems, as well as in electromagnetic compatibility and interference (EMC/EMI) problems [1]–[3]. Problems such as inefficiency and instability that used to cripple the TDIEs have been largely solved. Fast methods such as PWTD [4] and TD-AIM [5] have been developed and incorporated into TDIEs. For the late time instability problem, techniques such as the averaging/filtering method [6], exact integrations [7]–[9], smooth time basis functions [10], and Calderón preconditioning [11] have shown their effectiveness to obtain stable solutions.

Among the TDIEs, TD-EFIE is the most difficult to get stable solutions. Besides the internal resonance problem, which is a substantial cause of high-frequency instabilities, TD-EFIE also suffers from the low-frequency instabilities, which are due to TD-EFIE's null space of static solenoidal currents [10], [12]. Although difficult to stabilize, the TD-EFIE remains appealing for its high accuracy and versatility to open structures.

In [12], a loop-tree decomposition method for TD-EFIE is proposed to obtain a low-frequency stable marching on in time (MOT) solver. It is explained in [12] that augmenting the TD-EFIE with the first derivative of normal magnetic condition can effectively remedy the static currents. The test of the undifferentiated TD-EFIE using solenoidal basis functions has approximately the same efficacy, providing that the testing basis functions are suitably restricted [12]. In [13], the time-domain augmented electric field integral equation (TD-AEFIE) is proposed to cure the low-frequency instabilities, which originates from the frequency domain AEFIE for the low-frequency breakdown phenomenon [14]. A new set of charge density unknowns is added in the TD-AEFIE, which will inevitably increases the complexity, memory, and CPU time of the original TD-EFIE. In [15] and [16], the hierarchical approach is proposed to implement the quasi-Helmholtz decomposition. The hierarchical regularization has a good capability of dealing with the low-frequency breakdown phenomenon in the TD-EFIE. The use of hierarchical bases can yield well-conditioned MOT system matrices as the time step increases when analyzing quasi-static field interactions.

In this communication, we focus on the construction of a low-frequency stable TD-EFIE for general scattering problems not just for the quasi-static ones. The same testing scheme as in [12] is adopted, while the Helmholtz decomposition is implemented using the loop-flower basis functions, which have been proposed recently and applied effectively in the method of moment (MoM) for low-frequency break down problems and the Calderón preconditioning technique in [17]. This kind of decomposition avoids the search for tree basis and the degrees of freedom (DoF) can be compressed compared with that based on the Rao-Wilton-Glisson (RWG) or loop-tree/star basis functions [17]. To get a robust MOT solver, the averaging technique is also adopted here to eliminate the high-frequency oscillations, which is computationally efficient despite slight loss of accuracy.

II. Formulation

When a PEC scatterer, whose surface is S, is illuminated by an incident field $\boldsymbol{E}^{\mathrm{inc}}(\boldsymbol{r},t)$, surface currents $\boldsymbol{J}$ are induced and the standard TD-EFIE can be derived

$$T(\boldsymbol{J}) = -\hat{\boldsymbol{n}} \times \boldsymbol{E}^{\mathrm{inc}}(\boldsymbol{r},t) \tag{1}$$

in which $\boldsymbol{r}$ is the field point, $\hat{\boldsymbol{n}}$ represents the normal unit vector of S. The electric integral operator $T(\boldsymbol{J})$ can be written as

$$T(\boldsymbol{J}) = -\frac{\mu}{4\pi}\hat{\boldsymbol{n}} \times \int_{S'} \frac{\partial_t \boldsymbol{J}(\boldsymbol{r}', t - R/c)}{R} dS' + \frac{1}{4\pi\varepsilon}\hat{\boldsymbol{n}} \times \nabla \int_{S'} \frac{\int_{-\infty}^{t-R/c} \nabla_s' \cdot \boldsymbol{J}(\boldsymbol{r}', \tau)\, d\tau}{R} dS'. \tag{2}$$

Here, ∂_t denotes the first order time derivative, ε is permittivity, μ is permeability, c is the speed of light in free space, and $R = |\boldsymbol{r}' - \boldsymbol{r}|$.

Due to the time integral in $T(\boldsymbol{J})$, (1) is usually differentiated with respect to time

$$\partial_t T(\boldsymbol{J}) = -\hat{\boldsymbol{n}} \times \partial_t \boldsymbol{E}^{\mathrm{inc}}(\boldsymbol{r},t). \tag{3}$$

We will refer to (1) as the integral form of the TD-EFIE and (3) as the differentiated form.

In the following, we adopt the loop-flower basis functions to spatially discretize $T(\boldsymbol{J})$. A loop basis function is depicted in Fig. 1(a). It is defined with respect to the reference node $\boldsymbol{r}_n$, with support on all the triangles connecting to $\boldsymbol{r}_n$. A reference rotation direction is assigned for each loop basis function. A loop basis function can be expressed by the aggregation of RWG basis functions as follows:

$$\boldsymbol{f}_n^L(\boldsymbol{r}) = \sum_{i=1}^{N_n} \frac{C_n^L}{l_{n,i}} \boldsymbol{f}_{n,i}^R(\boldsymbol{r}) \tag{4}$$

where N_n is the number of the surrounding triangles, $\boldsymbol{f}_{n,i}^R(\boldsymbol{r})$ is the ith RWG basis whose common edge is connected to the node $\boldsymbol{r}_n$, and $l_{n,i}$ is the common edge length. $C_n^L = 1$ if $\boldsymbol{f}_{n,i}^R(\boldsymbol{r})$ is in the same direction

Manuscript received March 31, 2014; revised October 20, 2014; accepted December 22, 2014. Date of publication January 08, 2015; date of current version March 02, 2015. This work was supported in part by the SAST Foundation 2013 and in part by the National Science Foundation of China under Grant 61234001.

X. Tian and G. Xiao are with the Key Laboratory of Ministry of Education for Research of Design and EMC of High Speed Electronic Systems, Shanghai Jiao Tong University, Shanghai 200240, China (e-mail: smarter@sjtu.edu.cn).

J. Fang is with the Key Laboratory of Electromagnetic Environmental Effects for Aerospace Vehicle, Shanghai 200438, China.

Color versions of one or more of the figures in this communication are available online at http://ieeexplore.ieee.org.

Digital Object Identifier 10.1109/TAP.2015.2389247

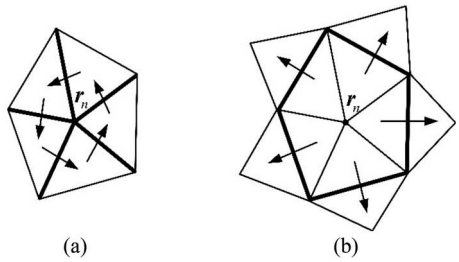

Fig. 1. (a) Loop basis function. (b) Flower basis function.

with the reference direction of the loop basis, otherwise, $C_n^L = -1$. The common edges of RWGs are plotted with bold lines in Fig. 1(a).

A flower basis function is also defined with respect to the reference node $\boldsymbol{r}_n$, and a reference direction is assigned for each flower basis function, as shown in Fig. 1(b). It can be explicitly expressed by

$$\boldsymbol{f}_n^F(\boldsymbol{r}) = \sum_{i=1}^{N_n} \frac{C_n^F}{l_{n,i}} \boldsymbol{f}_{n,i}^R(\boldsymbol{r}). \tag{5}$$

It can be checked that the loop basis functions are divergence-free, while the flower basis functions are approximately curl-free, which makes them suitable for performing the quasi-Helmholtz decomposition on a surface. The DoF of the loop and flower basis function has been fully discussed in [17]. The number of DoF of the loop and that of the flower basis functions on a qualified closed surface are both $N_n - 1$, where N_n is the number of nodes on the surface. For open structures, they are closely related to the number of internal nodes and RWG-connected node groups [17].

The surface current is divided into a solenoidal part $\boldsymbol{J}^L$ and a non-solenoidal part $\boldsymbol{J}^F$, expanded with loop-flower spatial basis functions, and Lagrange polynomial temporal basis functions as

$$\begin{aligned}\boldsymbol{J}(\boldsymbol{r},t) &= \boldsymbol{J}^L(\boldsymbol{r},t) + \boldsymbol{J}^F(\boldsymbol{r},t) \\ &= \sum_{j=1}^{N_t}\left[\sum_{n=1}^{N_n-1} \boldsymbol{I}_{n,j}^L \boldsymbol{f}_n^L(\boldsymbol{r}) T_j(t) + \sum_{n=1}^{N_n-1} I_{n,j}^F(t)\, \boldsymbol{f}_n^F(r)\, T_j(t)\right].\end{aligned} \tag{6}$$

Substituting (6) into (1) and (2), and applying the point matching in time and Galerkin testing in space, we can get a set of $N_t \times 2$ $(N_n - 1)$ matrix equations. Specifically, the integral form of TD-EFIE in (1) is tested with the loop function and the differentiated form in (2) is tested with the flower function. In such a spatial testing scheme, the integral term is avoided. Besides, the final matrix equation is equivalent to impose the differentiated normal magnetic condition on the original TD-EFIE [12], which can effectively eradicate the low-frequency instability. Finally, the matrix equation can be solved in the following marching form:

$$\begin{bmatrix} \boldsymbol{Z}_0^{\mathrm{LL}} & \boldsymbol{Z}_0^{\mathrm{LF}} \\ \boldsymbol{Z}_0^{\mathrm{FL}} & \boldsymbol{Z}_0^{\mathrm{FF}} \end{bmatrix} \begin{bmatrix} \boldsymbol{I}_j^L \\ \boldsymbol{I}_j^F \end{bmatrix} = \begin{bmatrix} \boldsymbol{V}_j^L \\ \boldsymbol{V}_j^F \end{bmatrix} - \sum_{k=1}^{N_t} \begin{bmatrix} \boldsymbol{Z}_k^{\mathrm{LL}} \boldsymbol{Z}_k^{\mathrm{LF}} \\ \boldsymbol{Z}_k^{\mathrm{FL}} \boldsymbol{Z}_k^{\mathrm{FF}} \end{bmatrix} \begin{bmatrix} \boldsymbol{I}_{j-k}^L \\ \boldsymbol{I}_{j-k}^F \end{bmatrix} \tag{7}$$

in which

$$V_{j,m}^L = \int_S \boldsymbol{f}_m^L(\boldsymbol{r}) \cdot \boldsymbol{E}^{\mathrm{in}}(\boldsymbol{r}, j\Delta t) dS \tag{8}$$

$$V_{j,m}^F = \int_S \boldsymbol{f}_m^F(\boldsymbol{r}) \cdot \partial_t \boldsymbol{E}^{\mathrm{in}}(\boldsymbol{r}, j\Delta t)\, dS \tag{9}$$

$$Z_{k,mn}^{\mathrm{LL}} = \frac{\mu}{4\pi} \int_S \boldsymbol{f}_m^L(\boldsymbol{r}) \cdot \int_{S'} \frac{\boldsymbol{f}_n^L(\boldsymbol{r}')\, \partial_t T(k\Delta t - R/c)}{R} dS' dS \tag{10}$$

$$Z_{k,mn}^{\mathrm{LF}} = \frac{\mu}{4\pi} \int_S \boldsymbol{f}_m^L(\boldsymbol{r}) \cdot \int_{S'} \frac{\boldsymbol{f}_n^F(\boldsymbol{r}')\, \partial_t T(k\Delta t - R/c)}{R} dS' dS \tag{11}$$

$$Z_{k,mn}^{\mathrm{FL}} = \frac{\mu}{4\pi} \int_S \boldsymbol{f}_m^L(\boldsymbol{r}) \cdot \int_{S'} \frac{\boldsymbol{f}_n^F(\boldsymbol{r}')\, \partial_t^2 T(k\Delta t - R/c)}{R} dS' dS \tag{12}$$

$$\begin{aligned}Z_{k,mn}^{\mathrm{Ff}} = {} & \frac{\mu}{4\pi} \int_S \boldsymbol{f}_m^L(\boldsymbol{r}) \cdot \int_{S'} \frac{\boldsymbol{f}_n^F(\boldsymbol{r}')\, \partial_t^2 T(k\Delta t - R/c)}{R} dS' dS \\ & + \frac{1}{4\pi\varepsilon} \int_S \nabla_s \cdot \boldsymbol{f}_m^F(\boldsymbol{r}) \int_{S'} \frac{\nabla_s' \cdot \boldsymbol{f}_n^F(r')\, T(k\Delta t - R/c)}{R} dS' dS.\end{aligned} \tag{13}$$

It is clear that the matrix entries are merely the linear combination of those in the RWG-based TD-EFIE. The implementation is straightforward from the original TD-EFIE [17].

The averaging technique has been proved to be an effective way to eliminate the high-frequency oscillation instabilities. Here, the commonly used three elements low-pass filtering scheme is adopted. The stability properties of the linear dynamic MOT system are closely related to the eigenvalues of its corresponding discrete systems [18]. The companion matrix of the averaged marching system can be found in [13]. If none of the companion matrix's eigenvalues falls out of the unit circle, the corresponding MOT system will be stable.

III. Numerical Results

The incident field is chosen as the modulated Gaussian plane wave, which can be written as

$$\boldsymbol{E}^{\mathrm{inc}}(\boldsymbol{r},t) = \hat{p} e^{-\gamma^2} \cos(2\pi f_0 \tau) \tag{14}$$

where $\gamma = (\tau - t_p)/(\sqrt{2}\sigma)$, $\tau = t - (\boldsymbol{r} \cdot \hat{k})/c$, $\sigma = 3/(2\pi f_{\mathrm{bw}})$, and $t_p = 8\sigma$. f_0 is the center frequency, f_{bw} is the bandwidth, and $f \in [f_0 - f_{\mathrm{bw}}, f_0 + f_{\mathrm{bw}}]$. $\hat{p}$ is the polarization of the incident wave and $\hat{k}$ is the direction of propagation. In all the numerical experiments, we set $\hat{p} = -\hat{x}$ and $\hat{k} = -\hat{z}$. For a reasonable time step, the temporal oversampling factor χ_o is introduced, which is defined as $\chi_o = 1/(2\Delta t f_{\max})$. In the following numerical experiments, the time basis is chosen as the third-order Lagrange polynomial function. Analytical expressions in [9] are used for the evaluation of the matrix elements. The matrix equations are solved using the Lower Upper (LU) decomposition and direct matrix inversion.

A. Sphere

In the first example, transient scattering from a PEC sphere with radius 0.5 m is analyzed. The surface mesh is composed of 152 triangles, 78 nodes, forming 228 RWGs. For the incident field, $f_0 = 50\,\mathrm{MHz}$, $f_{\mathrm{bw}} = 50\,\mathrm{MHz}$. The time step is 0.5 ns, $\chi_o = 10$.

Current coefficient of the labeled loop basis in 0–50 μs is depicted in Fig. 2. As the figure shows, the current decays exponentially after the incident vanishes and down to a floor at the order of -16. To validate the system's stability, the eigenvalues of its companion matrix are plotted in Fig. 3. We can see that the eigenvalues are all distributed inside the unit circle except those at $(1,\ 0i)$. There is a cluster of eigenvalues residing at $(1,\ 0i)$, and the zoomed-in Fig. 3(b) shows that they locate exactly on the unit circle at $(0,\ 0i)$, implying the low-frequency stable property.

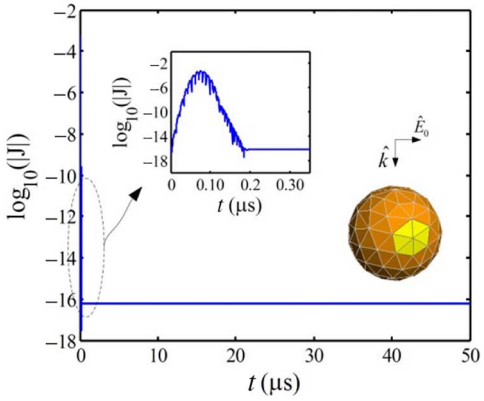

Fig. 2. Current coefficients of the observed loop on the sphere.

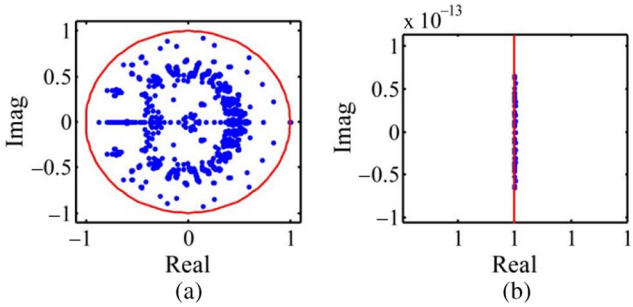

Fig. 3. (a) Eigenvalues of the MOT system for the sphere. (b) Zoomed-in at $(1,\ 0i)$.

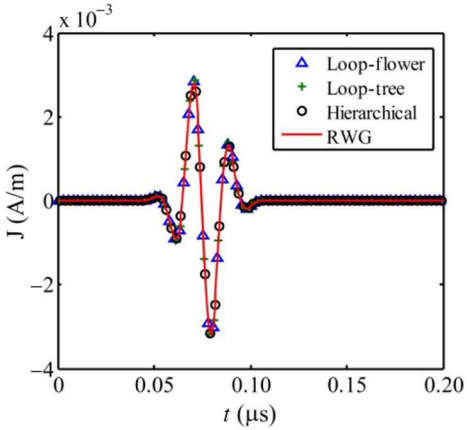

Fig. 4. Current density of an RWG on the sphere obtained using different bases.

To investigate the performance compared with the hierarchical approach, we construct a level-2 mesh by bisecting each edge of the original mesh and connecting the new nodes, as detailed in [15] and [19]. The set of hierarchical basis function of the coarse level is the loop-tree function. The scheme stated in [12] using the loop-tree function is also introduced here for comparison. The temporal bases are all chosen to be the third-order Lagrange polynomials. Under the excitation whose $f_0 = 50\,\mathrm{MHz}$ and $f_{\mathrm{bw}} = 50\,\mathrm{MHz}$, the currents obtained by different schemes are compared with the original RWG-based solutions in Fig. 4. The solutions are practically the same, clearly demonstrating the accuracy of different schemes.

To investigate the low-frequency performances of different solvers, the frequency varies from 1.0 GHz to 0.01 kHz and the oversampling factor remains to be 10. The average mesh edge size is 1/3 of the wavelength at 1.0 GHz. Fig. 5 shows the condition number of the MOT matrices constructed using the loop-flower, loop-tree, hierarchical, and

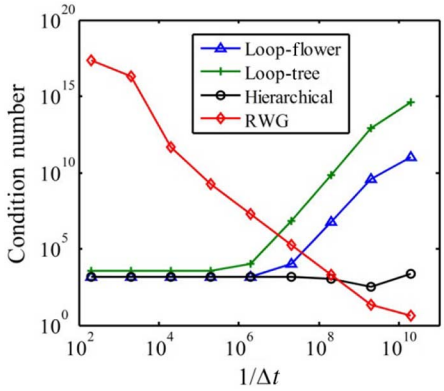

Fig. 5. Condition number of the MOT system matrices constructed using different bases and different time steps for the sphere.

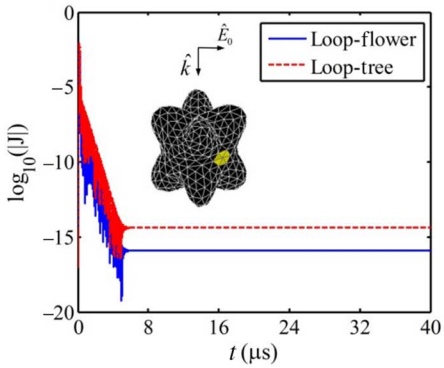

Fig. 6. Current coefficients of the observed loop basis on the smooth flower.

RWG bases. As frequency goes down, the matrices constructed using the RWG become increasingly ill-conditioned, whereas the matrices based on the loop-tree, loop-flower, and hierarchical bases have a constant condition number. The performance of the loop-flower basis at low frequency is better that of the loop-tree and quite near to that of the second-level hierarchical bases. But the RWG outperforms all these loop-separated bases at high frequencies.

B. Smooth Flower

Transient scattering from the flower shaped scatterer is discussed in this example. Its surface can be explicitly expressed by

$$r(\theta,\phi) = \sin^2(2\theta)\cos^2(\phi) + 1.5\ \mathrm{m}. \tag{15}$$

The mesh of the model is composed of 726 triangles, 365 nodes, 1089 RWGs. The center frequency of the incident is 50 MHz and the bandwidth is 20 MHz. The time step is chosen as 0.4 ns. The corresponding oversampling factor is 18. For this analysis, we employ both the loop-flower-based scheme and loop-tree-based scheme proposed in [12].

Fig. 6 shows the evolution of the current coefficient of the labeled loop basis in 100 000 time steps. We can see clearly that the current magnitudes converge exponentially in both schemes. Radar cross section (RCS) data sets at 50 and 70 MHz are compared with that obtained by the RWG-based MoM in Fig. 7. At 50 MHz, the mean relative one-normal errors [10] using loop-flower and loop-tree are 0.012 and 0.017, respectively, showing excellent accuracy of the MOT solvers.

C. Two Parallel Plates

In the following example, we apply the loop-flower basis functions to analyze scattering from open surfaces: two parallel PEC plates.

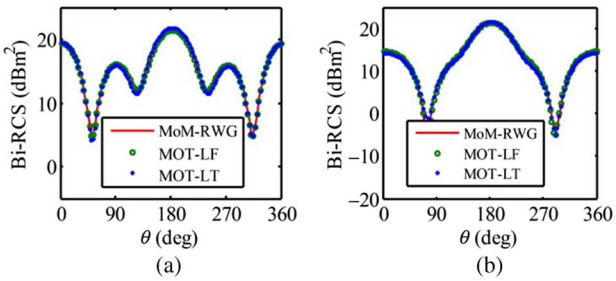

Fig. 7. Comparison of bistatic RCSs obtained by MOT and MoM solvers for the smooth flower at (a) 50 MHz; (b) 70 MHz.

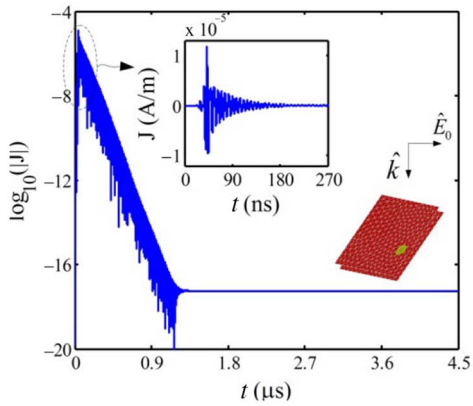

Fig. 8. Current coefficient of the observed loop on the parallel plate.

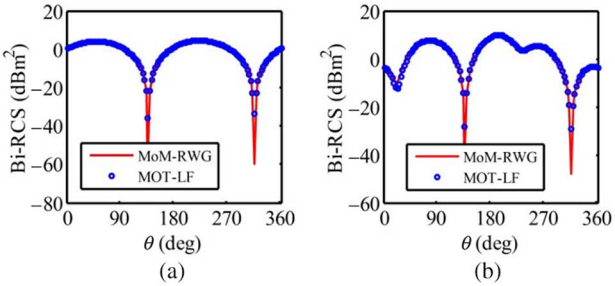

Fig. 9. Comparison of bistatic RCSs obtained by the MOT and MoM solvers for the parallel plate at (a) 100 MHz; (b) 250 MHz.

Both plates are of size $1\,\mathrm{m} \times 1\,\mathrm{m}$ and they are separated by 0.1 m. The structure is centered at origin of the coordinate, leaning 45° from the *X*–*Y* plane to *Y*–*Z* plane. Each plate is meshed with 256 nodes (including 200 inner nodes), 653 RWGs, resulting in 199 loop, and 255 flower basis functions. The excitation parameters are $f_0 = 200\,\mathrm{MHz}$ and $f_{\mathrm{bw}} = 100\,\mathrm{MHz}$. The time step is chosen as 0.09 ns, corresponding to $\chi_o = 19$.

Stable electric current of the observed loop basis is plotted in Fig. 8. There is a long tail in the temporal waveform, which is caused by the multiple reflections between the two plates. RCS data obtained by loop-flower-based MOT solver is compared with that computed by RWG-based MoM at 100 and 250 MHz in Fig. 9. The relative error at 100 and 250 MHz is 0.037 and 0.065, respectively, verifying the capability of the loop-flower basis functions for transient analysis of open structures.

IV. Conclusion

Loop-flower basis functions are adopted for a low-frequency stable MOT TD-EFIE solver. By performing the Helmholtz decomposition and combining the integral form with the differentiated form of the TD-EFIE, the low-frequency instability is eradicated. Compared to the loop-tree/star-based TD-EFIE, the unknowns are approximately 1/3 fewer for closed surfaces. The proposed MOT solver also has a good low-frequency performance. Numerical examples show that the proposed method is stable and accurate for both open and closed structures.

References

[1] S. M. Rao, D. R. Wilton, and A. W. Glisson, "Electromagnetic scattering by surfaces of arbitrary shape," *IEEE Trans. Antennas Propag.*, vol. AP-30, no. 5, pp. 409–418, May 1982.

[2] T. K. Sarkar, W. Lee, and S. M. Rao, "Analysis of transient scattering from composite arbitrarily shaped complex structures," *IEEE Trans. Antennas Propag.*, vol. 48, no. 10, pp. 1625–1634, Oct. 2000.

[3] H. Bagcı, A. E. Yılmaz, J. M. Jin, and E. Michielssen, "Fast and rigorous analysis of EMC/EMI phenomena on electrically large and complex cableloaded structure," *IEEE Trans. Electromagn. Compat.*, vol. 49, no. 2, pp. 361–381, May 2007.

[4] B. Shanker, A. Arif Ergin, M. Lu, and E. Michielssen, "Fast analysis of transient scattering phenomena using the multilevel plane wave time domain algorithm," *IEEE Trans. Antennas Propag.*, vol. 51, no. 3, pp. 628–641, Mar. 2003.

[5] A. E. Yilmaz, J. M. Jin, and E. Michielssen, "Time domain adaptive integral method for surface integral equations," *IEEE Trans. Antennas Propag.*, vol. 52, no. 10, pp. 2692–2708, Oct. 2004.

[6] A. Sadigh and E. Arvas, "Treating the instabilities in marching-on-intime method from a different perspective," *IEEE Trans. Antennas Propag.*, vol. 41, no. 12, pp. 1695–1702, Dec. 1993.

[7] Y. Shi, M. Xia, R. Chen, E. Michielssen, and M. Lu, "Stable electric field TDIE solvers via quasi-exact evaluation of MOT matrix elements," *IEEE Trans. Antennas Propag.*, vol. 59, no. 2, pp. 574–585, Feb. 2011.

[8] H. A. Ülkü and A. A. Ergin, "Application of analytical retarded-time potential expressions to the solution of time domain integral equations," *IEEE Trans. Antennas Propag.*, vol. 59, no. 11, pp. 4123–4131, Nov. 2011.

[9] X. Tian, G. Xiao, and S. Xiang, "Application of analytical expressions for retarded-time potentials in analyzing the transient scattering by dielectric objects," *IEEE Antennas Wireless Propag. Lett.*, vol. 13, pp. 1313–1316, Jun. 2014.

[10] D. S. Weile, G. Pisharody, N.-W. Chen, B. Shanker, and E. Michielssen, "A novel scheme for the solution of the time-domain integral equations of electromagnetics," *IEEE Trans. Antennas Propag.*, vol. 52, no. 1, pp. 283–295, Jan. 2004.

[11] F. P. Andriulli, K. Cools, F. Olyslager, and E. Michielssen, "Time domain Calderón identities and their application to the integral equation analysis of scattering by PEC objects Part II: Stability," *IEEE Trans. Antennas Propag.*, vol. 57, no. 8, pp. 2365–2375, Aug. 2009.

[12] G. Pisharody and D. S. Weile, "Robust solution of time-domain integral equations using loop-tree decomposition and bandlimited extrapolation," *IEEE Trans. Antennas Propag.*, vol. 53, no. 6, pp. 2089–2098, Jun. 2005.

[13] X. Tian and G. Xiao, "Time-domain augmented electric field integral equation for a robust marching on in time solver," *IET Microw. Antennas Propag.*, vol. 8, no. 9, pp. 688–694, Jun. 2014.

[14] Z. Qian and W. Chew, "Fast full-wave surface integral equation solver for multiscale structure modeling," *IEEE Trans. Antennas Propag.*, vol. 57, no. 11, pp. 3594–3602, Nov. 2009.

[15] F. P. Andriulli, H. Bagci, F. Vipiana, G. Vecchi, and E. Michielssen, "A marching-on-in-time hierarchical scheme for the solution of the time domain electric field integral equation," *IEEE Trans. Antennas Propag.*, vol. 55, no. 12, pp. 3734–3738, Dec. 2007.

[16] F. P. Andriulli, H. Bagci, F. Vipiana, G. Vecchi, and E. Michielssen, "Analysis and regularization of the TD-EFIE low-frequency breakdown," *IEEE Trans. Antennas Propag.*, vol. 57, no. 7, pp. 2034–2046, Jul. 2009.

[17] G. Xiao, "Applying loop-flower basis functions to analyze electromagnetic scattering problems of PEC scatterers," *Int. J. Antennas Propag.*, vol. 2014, 9 pp., 2014, article ID 905935.

[18] S. P. Walker, M. J. Bluck, and I. Chatzis, "The stability of integral equation time domain computations for three-dimensional scattering; similarities and differences between electrodynamic and elastodynamic computations," *Int. J. Numer. Model.*, vol. 15, pp. 459–474, 2000.

[19] F. Vipiana, P. Pirinoli, and G. Vecchi, "A multi-resolution method of moments for triangular meshes," *IEEE Trans. Antennas Propag.*, vol. 53, no. 7, pp. 2247–2258, Jul. 2005.